Manganese Superoxide Dismutase Enhances the Invasive and Migratory Activity of Tumor Cells

Kip M. Connor,[1] Nadine Hempel,[1] Kristin K. Nelson,[1] Ganary Dabiri,[2] Aldo Gamarra,[1] James Belarmino,[3,4] Livingston Van De Water,[2] Badar M. Mian,[1,3,4] and J. Andres Melendez[1]

Centers for [1]Immunology and Microbial Disease and [2]Cell Biology and Cancer Research and [3]Division of Urology, Albany Medical College and [4]Stratton Veterans Affairs Medical Center, Albany, New York

Abstract

Clinically significant elevations in the expression of manganese superoxide dismutase (Sod2) are associated with an increased frequency of tumor invasion and metastasis in certain cancers. The aim of this study was to examine whether increases in Sod2 activity modulate the migratory potential of tumor cells, contributing to their enhanced metastatic behavior. Overexpression of Sod2 in HT-1080 fibrosarcoma cells significantly enhanced their migration 2-fold in a wound healing assay and their invasive potential 3-fold in a transwell invasion assay. Severity of invasion was directly correlated to Sod2 expression levels and this invasive phenotype was similarly observed in 253J bladder tumor cells, in which Sod expression resulted in a 3-fold increase in invasion compared with controls. Further, migration and invasion of the Sod2-expressing cells was inhibited following overexpression of catalase, indicating that the promigratory/invasive phenotype of Sod2-expressing cells is H_2O_2 dependent. Sod2 overexpression was associated with a loss of vinculin-positive focal adhesions that were recovered in cells coexpressing catalase. Tail vein injections of Sod2-GFP–expressing HT-1080 cells in NCR nude mice led to the development of pulmonary metastatic nodules displaying high Sod2-GFP expression. Isolated tumors were shown to retain high Sod2 activity in culture and elevated levels of the matrix degrading protein matrix metalloproteinase-1, and a promigratory phenotype was observed in a population of cells growing out from the tumor nodule. These findings suggest that the association between increased Sod2 activity and poor prognosis in cancer can be attributed to alterations in their migratory and invasive capacity. [Cancer Res 2007; 67(21):10260–67]

Introduction

A hallmark of malignancy and a primary cause of morbidity and mortality in cancer patients is metastasis. Tumor metastasis is a multistep process initiated by migration and invasion of cells into the surrounding vasculature. This is followed by extravasation from the circulation and proliferation at a secondary site where the formation of a metastatic lesion occurs (1). A key process in the initial movement and subsequent invasion of neoplastic cells into the circulatory system is the remodeling of the extracellular matrix (2). Whereas the complete mechanism by which migration and invasion occurs is not completely defined, further insight into the regulation of this cascade of events may allow for novel therapeutic strategies.

Emerging evidence has implicated reactive oxygen species (ROS) and the activation of redox-sensitive signaling pathways in invasion and migration (3–6). Intrinsic antioxidant enzymes are vital to the regulation of oxidative stress within cells. Of these, one of the primary cellular antioxidants, superoxide dismutase (Sod), catalyzes the conversion of superoxide ($O_2^{\cdot-}$) to hydrogen peroxide (H_2O_2), which can then be removed by catalase (CAT), glutathione peroxidase, or peroxiredoxins. *In vitro* studies have shown that a number of cancer cell lines contain elevated levels of mitochondrial manganese-containing superoxide dismutase (Sod2) and decreased levels of CAT, and that this change in steady-state levels of H_2O_2 correlates with increased metastasis, proliferation, and resistance to apoptosis (7, 8). Epidemiologic evidence has also linked a single nucleotide polymorphism in *Sod2*, which increases its activity, to risk of developing breast (9) and prostate (10) cancers.

An essential and rate-limiting step in metastasis is the remodeling and degradation of the extracellular matrix and basement membrane by proteolytic enzymes (11–13). In this model, cells must interact with surrounding stromal cells, leading to the loss of matrix function and resulting in a compromised matrix boundary (11–13). Matrix metalloproteinases (MMP) are major contributors of stromal degradation and are vital to the process of cellular invasion (12). MMP-1/interstitial collagenase has a specificity for type I collagen, the primary collagen of the interstitial matrix (13), although it has been shown to degrade collagen types II, III, VII, and X (13). Studies using antisense mRNA against MMP-1 in melanoma cells have shown a significant attenuation in the capacity of these cells to invade type I collagen and Matrigel *in vitro* (14). Moreover, the expression of MMP-1 has been shown to be a definitive prognostic marker for breast lesions that will develop into cancer and (15) and suggests that the expression and regulation of MMP-1 may be important in malignancy.

Studies from this and other laboratories have shown that the Sod2-dependent production of H_2O_2 leads to increased expression of MMP family members and that there is a strong correlation between this increase in MMP levels and enhanced metastasis (11, 16–19). Interestingly, the Sod2-dependent increases in MMP expression can be reversed by the H_2O_2-detoxifying enzyme CAT

Note: Supplementary data for this article are available at Cancer Research Online (http://cancerres.aacrjournals.org/).

K.M. Connor and N. Hempel contributed equally to this work. Current address for K.K. Nelson: James Graham Brown Cancer Center, Baxter II Biomedical Research Building, University of Louisville, 580 South Preston Street, Louisville, KY 40202. Current address for K.M. Connor: Department of Ophthalmology, Children's Hospital Boston, Harvard Medical School, 1 Blackfan Circle, Boston, MA 02115.

Requests for reprints: J. Andres Melendez, Center for Immunology and Microbial Disease MC151, Albany Medical College, 47, New Scotland Avenue, Albany, NY 12208. Phone: 518-262-8791; Fax: 518-262-6161; E-mail: melenda@mail.amc.edu.

doi:10.1158/0008-5472.CAN-07-1204

or glutathione peroxidase (16–18). Thus, Sod2-dependent up-regulation of MMPs may, in part, contribute to increased invasion and metastatic capacity of tumors displaying elevated Sod2 levels (16, 18).

In this study, we tested the hypothesis that the Sod2-dependent production of H_2O_2 can influence the invasive and migratory properties of tumor cell lines. We used both *in vitro* and *in vivo* methods to examine the role of Sod2 in invasion and migration. Our findings suggest that increases in mitochondrial H_2O_2 by Sod2 can enhance the invasive and migratory properties of tumor cells and that efficient H_2O_2 detoxification may restrict the metastatic phenotype.

Materials and Methods

Cell culture and reagents. Human HT-1080 fibrosarcoma and 253J transitional bladder carcinoma cell lines were maintained in MEM containing 10% FCS, 1,000 units/mL penicillin, and 500 μg/mL streptomycin in a 37°C incubator containing 5% CO_2. Recombinant Sod2 and catalase plasmid constructs were synthesized and transfected as previously described (20, 21). Briefly, HT-1080 cells were transfected with the pEGFPN1-MnSOD construct (provided by Dr. Sonia Flores, Webb-Waring Institute for Cancer, Aging, and Antioxidant Research, University of Colorado Health Science Center, Denver, CO) using LipofectAMINE Plus reagent according to the manufacturer's specifications and cells were cultured in selective medium containing 1 mg/mL neomycin. The catalytically inactive mutant of Sod2 (ΔSod2) was previously described and characterized by Nelson et al. (22). Cells were sorted based on green fluorescent protein (GFP) fluorescence as described by Connor et al. (23).

Wound healing assay. Cells were grown to confluence and wounded by dragging a 1-mL pipette tip through the monolayer. Cells were washed to remove cellular debris and allowed to migrate for 24 h. Images were taken at time 0 and 24 h post-wounding under a Nikon Diaphot TMD inverted microscope (20×). The relative distance traveled by the leading edge from 0 to 24 h was assessed using Photoshop 7.0 software ($n = 6$).

Transwell invasion assay. Biocoat Matrigel invasion chamber inserts (BD Biosciences) were equilibrated for 2 h at 37°C in serum-free medium. GFP, Sod2-GFP^{lo}, and Sod2-GFP^{hi} stably expressing cell lines were seeded at a density of 2.5×10^4 per well in serum-free medium in the upper chamber of the insert and cells were allowed to invade through the Matrigel for 22 h at 37°C with 5% CO_2, using medium containing 10% fetal bovine serum (FBS) in the lower chamber as a chemoattractant. Following migration, cells were washed with PBS and fixed with 3% formaldehyde/PBS for 15 min. Following washing with PBS, cells in the upper chamber were removed with a cotton swab and cells on the bottom surface of the filter were rinsed and permeabilized with 1% Triton X-100 in PBS for 20 min. Cells were stained with Hoechst 33258 (1 μg/mL) for 30 min in the dark and visualized under a fluorescent microscope. Three random fields were captured at ×10 magnification ($n = 3$).

Vinculin/focal contact staining. Cells were prepared and stained, and images were analyzed essentially as described by Dabiri et al. (24). In brief, cells were maintained in complete medium, grown to subconfluence, washed, formaldehyde fixed, permeabilized, and blocked with 2% bovine serum albumin (BSA). All primary and secondary antibodies were diluted in 2% BSA/PBS as previously described.

***In vivo* metastatic xenograft model.** Sod2-GFP–positive cells (1×10^6) were injected into the tail veins of male NCR athymic mice at 3 to 4 weeks of age (Taconic). Two months postinjection, mice were sacrificed and cross sections of lungs viewed under a fluorescent microscope to visualize GFP-positive pulmonary tumor nodules. Pulmonary tumor nodules were also resected from lungs and placed into cell culture. A sublayer of tumor cells was allowed to grow from the resected tumor and then photographed under a fluorescent microscope. Lung tissue harvested from nude mice was rapidly frozen in optimum cutting temperature embedding compound (Triangle Biomedical) and stored at −70°C until cryosections (~10 mm) were collected on gelatinized slides. All slides/coverslips were washed twice in PBS and then incubated in 3.7% formaldehyde at 37°C for 10 min.

Time-lapse video microscopy. Stably transfected Sod2-GFP cells were injected into the tail veins of nude mice as described above. Pulmonary metastatic nodules were resected and brightly GFP fluorescing nodules allowed to grow in culture in MEM supplemented with 10% FBS, 1,000 units/mL penicillin, 500 μg/mL streptomycin, and 1 mg/mL neomycin in a 37°C incubator containing 5% CO_2. After a week of growth in culture, the migratory capacity of the cells at the leading edge of the outgrowth of cells underlying the tumor nodule was monitored for 24 h. HEPES (25 mmol/L, pH 7.3) was added to the media to maintain pH. Phase-contrast, epifluoresence, and time-lapse video microscopic analyses of live cells were conducted with an Olympus I × 70 inverted microscope at low magnification using a 10× dry objective lens. Images were captured using a Peltier cooled charge-coupled device Cooke SensiCam High Performance camera (Cooke Corporation) and Image ProPlus software (Media Cybernetics). Live transfected cells overexpressing GFP constructs were located by fluorescence and imaged by time-lapse video phase-contrast microscopy to document the movement of cells from the underlying monolayer of the resected tumor nodule. Digital time-lapse videos of cells were recorded with images collected at 10-min intervals over a period of 24 h. The distance moved by the cells was measured using ImageJ software. Cells were sorted based on fluorescence intensity. Nine brightly and nine dimly fluorescing cells were selected and their paths were traced through x and y coordinates within the imaging field. Relative distance migrated was calculated using the following formula: $\Sigma(x_{t_{n+1}} + x_{t_n})^2 + (y_{t_{n+1}} + y_{t_n})^2$, where x and y indicate coordinates measured at each indicated time interval (t). Statistical analysis was conducted using the two-sample t test with a 95% confidence interval.

MMP-1 immunoprecipitation and immunoblotting. Control (CMV) and Sod2-overexpressing cells were grown to confluence and media analyzed for MMP-1 protein expression by Western blotting. Complete media from the cells were normalized to cell count and resuspended with 50 μL of heparin sepharose beads (Amersham Pharmacia Biotech) overnight at 4°C in a rotating incubator. The MMP-1–conjugated beads were centrifuged at 1,000 rpm for 5 min and boiled for 5 min with HBSS and 5× loading dye containing 5% 2-mercaptoethanol. The beads were again centrifuged and the supernatant was loaded on a 10% PAGE and transferred onto a nitrocellulose membrane (Bio-Rad) at 100 V for 1 h. The membranes were blocked with primary monoclonal MMP-1 antibody (R&D Systems) at 1:400 in TBS containing 0.1% Tween 20 and 5% milk, washed, and then incubated with secondary antibody (horseradish peroxidase–conjugated antimouse immunoglobulin) at 1:4,000 for 1 h at room temperature (Amersham Pharmacia Biotech). Protein detection was done by the addition of Pierce SuperSignal Chemiluminescent Substrate for 5 min and the immunoblot was exposed to Kodak MS radiographic film (Kodak).

MMP-1, tissue inhibitor of metalloproteinase-1, and tissue inhibitor of metalloproteinase-2 real-time reverse transcription-PCR. RNA was extracted as previously described (25) and primer sequences, optimal annealing temperatures, and PCR product size are as follows: *MMP-1* (55°C, 550 bp), 5′-GGAGGAAATCTTGCTCAT, 3′-CTCAGAAAGAGCAGCATC; tissue inhibitor of metalloproteinase-1 (*TIMP-1*; 56°C, 138 bp), 5′-CAGCGACGAGTTTCTCATTGCT-3′, 3′-GTTCTGGATGTGACAACCGACACT-5′; *TIMP-2* (56.6°C, 242 bp), 5′-GTGAGAAGGAAGTGGACTGAAAC-3′, 3′-TAGTGGGAGACACTGAAGTAGCAC-5′. B was the control (55.0°C, 580 bp), 5′-ACCAACTGGGACGACATGGAGAAA-3′, 5′-TAGCACAGCCTGGATAGCAACGTA-3′. The iQ SYBR Green supermix was used for real-time PCR. The 2× supermix contains 100 mmol/L KCl, 40 mmol/L Tris-HCl, (pH 8.4), 0.4 mmol/L each of deoxynucleotide triphosphates (dATP, dCTP, dGTP, and dTTP), 50 units/mL hot-start iTaq DNA polymerase, 6 mmol/L $MgCl_2$, SYBR Green I dye, and 20 nmol/L fluorescein. The real-time PCR mixture (20 μL) consisted of 7.4 μL distilled H_2O, 10.0 μL SYBR Green, 1.0 μL cDNA, 0.8 μL forward primer, and 0.8 μL reverse primer for each cell line and for each primer set being investigated. Amplification was carried out by MyiQ Single Color Real-time PCR Detection System. The Amplification process consisted of five cycles: cycle 1, 94.0°C for 03:00 min; cycle 2, 41 cycles of 94.0°C for 30 s, primer-specific annealing temperature (PS °C) for 30 s, and 72.0°C for 30 s;

cycle 3, 95.0°C for 1 min; cycle 4, PS °C for 1 min; and cycle 5, 80 cycles of PS °C for 10 s. Melting curve data were collected and analyzed with the MyiQ software. Each experiment was done in triplicate and normalized to β-actin. To determine the quantity of the target gene-specific transcripts present in cells, their respective C_t values were first normalized by subtracting the C_t value obtained from the β-actin control ($\Delta C_t = C_{t,\ target} - C_{t,\ control}$). The relative concentration of gene-specific mRNA was determined using the formula $2^{-\Delta\Delta C_t}$, where $-\Delta\Delta C_t = \Delta C_{t(sample)} - \Delta C_{t(\beta\text{-actin})}$.

Sod zymography. The determination of Sod activity was done as previously described (26). Briefly, the indicated cell lines were lysed and 10 μg of whole-cell lysates were separated on a 10% nondenaturing PAGE for ~2 h at 110 V. The gel was incubated in 0.125 mmol/L nitroblue tetrazolium, 0.4 μmol/L riboflavin, 0.075 mmol/L TEMED, and 50 mmol/L potassium phosphate (pH 7.8)/0.1 mmol/L EDTA for 15 min in the dark. The gel was rinsed in water and exposed to light to visualize the bands representing Sod activity.

Statistical analysis. ANOVA with $\alpha = 0.05$ was used for processing the data. A two-sample t test was used as posttest unless otherwise indicated.

Results

Sod2 promotes wound closure and is H_2O_2 dependent. Migration and invasion present two important aspects that lead to the ability of cancer cells to form metastases. In an effort to further characterize the role of Sod2 in aiding metastasis, we investigated the role of Sod2 in migration using a classic wound healing assay. Whereas overexpression of a mitochondrially-targeted GFP construct failed to promote sheet migration of HT-1080 cells into the monolayer wounds, Sod2-GFP–expressing cells displayed enhanced migration and closure of the wound in the same 24-h time frame (Fig. 1*A*). Moreover, highest expression of Sod2 was observed in those cells found at the leading edge of cells migrating into the wound. Further, we sought to analyze the migratory properties of HT-1080 cells that have been redox engineered to modulate H_2O_2 levels by stable overexpression of Sod2 and CAT. Whereas Sod2 overexpression results in an increase in H_2O_2, this increase can be reversed by expressing the H_2O_2-detoxifying enzyme CAT (21). Similar to results of Fig. 1*A*, Sod2 overexpression caused a significant increase in migration in the wound healing model. Sod2-expressing cells migrated at double the rate of empty vector–transfected cells (CMV; Fig. 1*B* and *C*), whereas a catalytically inactive mutant of Sod2 (ΔSod2) had no effect on cellular migration when stably transfected in HT-1080 cells (Fig. 1*D*). Coexpression of CAT resulted in abrogation of the Sod2-dependent increase of wound closure (Fig. 1*C*), displaying a lack of migration similar to that of the control cells. Cells overexpressing only CAT showed a similar rate of wound closure as control cells (data not shown). This suggests that H_2O_2 production is required for the promigratory effects observed following Sod2 overexpression.

Sod2 augments cell invasion. A critical component of tumor metastasis is invasion of the tumor cell through the basement membrane and into the surrounding stroma. To evaluate the role of increased Sod2 expression in tumor cell invasion, we used a transwell invasion assay. Cells with low and high levels of Sod2-GFP fusion protein (Sod2-GFP^{lo} and Sod2-GFP^{hi}) were allowed to invade through a Matrigel matrix using medium supplemented with FBS as the chemoattractant. The HT-1080 Sod2-GFP–expressing cells have previously been characterized *in vitro* and were shown to display Sod2-GFP fluorescence that is directly correlated with the level of intracellular Sod2 activity (23). Sod2-GFP^{lo} and Sod2-GFP^{hi} expressing HT-1080 cells were shown to display ~2.5- and 4.4-fold higher Sod activity, respectively, compared with GFP only–expressing control cells, according to Sod zymography activity assay (23). The levels of Sod2 expression correlated with an increase in the invasive properties of these cell lines (Fig. 2*A*). These data suggest that increases in Sod2 expression may play a key role in the acquisition of the ability to invade basement membrane barriers.

The ability of Sod2 overexpression to modulate invasion is not restricted to HT-1080 fibrosarcoma cell lines and was also observed in 253J transitional bladder carcinoma cells (Fig. 2*B*). In addition, the proinvasive phenotype following Sod2 expression in the bladder carcinoma cells was similarly reversed by coexpression of CAT,

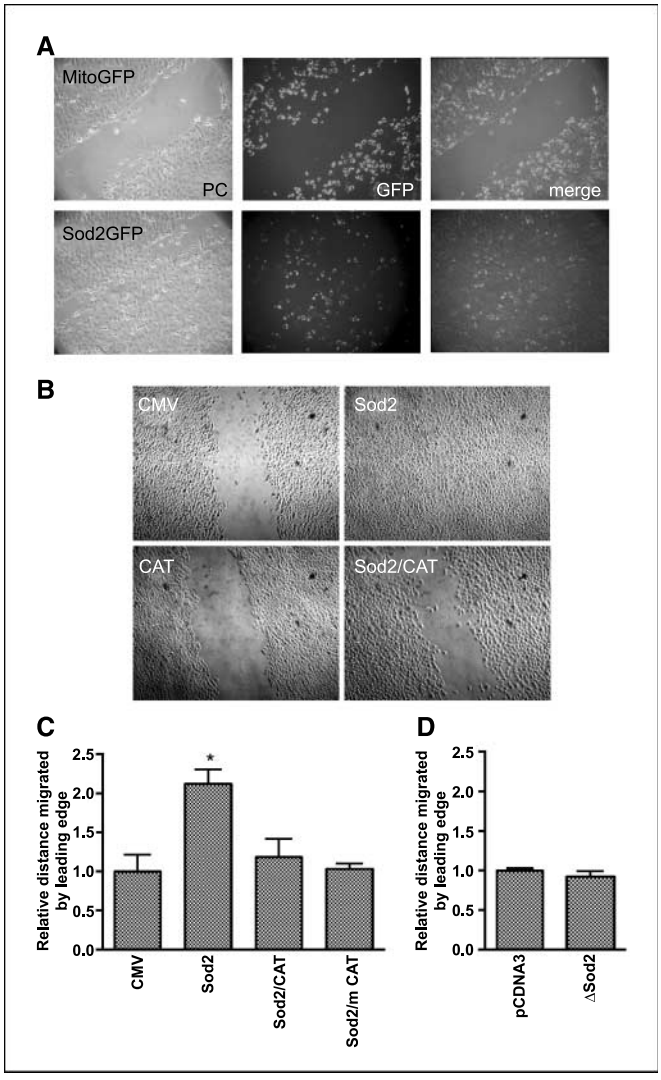

Figure 1. Sod2-dependent production of H_2O_2 results in increased migration. *A,* expression of Sod2 promotes migration of HT-1080 cells in a wound healing assay. HT-1080 cells were stably transfected with mitochondrially-targeted GFP or Sod2-GFP. The confluent monolayer was wounded with sterile pipette tip and cells were allowed to migrate for 24 h. Phase-contrast (*PC*) and fluorescence images (*GFP*) of the cells were taken 24 h post wounding. *B,* the promigratory effects of Sod2 are inhibited by coexpression of CAT. Redox-engineered HT-1080 cells (Sod2-, CAT-, Sod2/CAT–, and empty vector CMV–transfected cells) were seeded to confluence and wounded. Representative images at 24 h post wounding. *C,* quantification of distance migrated by redox-engineered HT-1080 cell lines from time 0 to 24 h relative to control cells (CMV); $n = 6$. Sod2-transfected cells displayed significantly more migration than control cells. *, $P \leq 0.05$. *D,* quantification of distance migrated by HT-1080 cells stably expressing mutant inactive Sod2 (*ΔSod2*) relative to control cells (*pCDNA3*); $n = 6$.

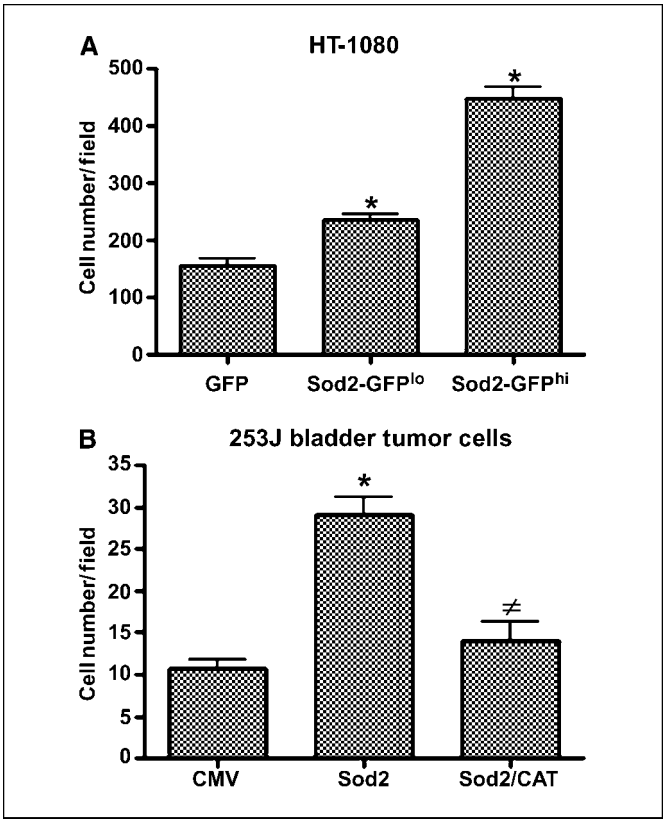

Figure 2. Sod2 expression enhances the invasive phenotype of HT-1080 and bladder tumor cells. Control (GFP), Sod2-GFP^{lo}, and Sod2-GFP^{hi} HT-1080 cells (*A*) or 253J bladder tumor cells transfected with empty CMV vector, Sod2, or Sod2 with CAT (*B*) were seeded in serum-free medium in a BD Biocoat Matrigel invasion chamber. Cells were allowed to invade through the Matrigel toward the lower chamber containing medium supplemented with FBS as a chemoattractant for 22 h. The number of cells invading through the chamber was quantified for each of the indicated cell lines. *, $P \leq 0.0001$, significant difference in invasion compared with control.

showing that the invasion mediated by Sod2 in 253J cells is H_2O_2 dependent.

Sod2 expression leads to a loss of focal adhesions. To further characterize the cellular phenotype associated with Sod2-induced migration, the morphologic changes in redox-engineered cells were investigated. Compared with vector only–transfected cells (CMV), HT-1080 cells expressing Sod2 displayed a more spindle-like morphology, with visible protrusions suggestive of lamellipodia (Fig. 3). This morphologic change was further highlighted when assessing the presence of focal adhesions by immunofluorescent staining for vinculin. HT-1080-CMV cells exhibited broadly distributed focal adhesions, indicative of adherent nonmotile cells, whereas HT-1080-Sod2 cells exhibited a striking loss of this wide vinculin staining (Fig. 3). Some cells expressing Sod2 exhibited limited but targeted staining for vinculin at distinct regions indicative of leading edge focal complexes, which is a common feature of migrating cells (Fig. 3, *arrow*). On coexpression of CAT, this phenotype was reversed, with clear vinculin staining similar to that observed in the control cells (Fig. 3), suggesting that the loss of focal adhesions is H_2O_2 dependent.

Enforced Sod2-GFP expression promotes lung metastasis and is retained in isolated tumor cells from metastatic lesions. Previous *in vivo* studies have shown that the metastatic capacity of HT-1080 fibrosarcoma cells is enhanced when Sod2 is overexpressed (16). To further characterize the phenotypic changes that contribute to this increase in metastatic potential, the *in vivo* metastatic capacity of a stable population of Sod2-GFP–overexpressing HT-1080 fibrosarcoma cells was monitored. The cells were tail vein injected into nude mice and lung cryosections analyzed for GFP fluorescence when mice were sacrificed 2 months postinjection, providing a useful tool for the visualization of intrapulmonary micrometastases derived from single tumor cells (Fig. 4*A*). Mice injected with Sod2-GFP–transfected HT-1080 cells presented with multiple intrapulmonary metastatic lesions surrounding pulmonary blood vessels (Fig. 4*A*). On sacrifice, several tumor nodules from the mice were resected and placed in cell culture. The tumor nodules retained high GFP intensity after growth in cell culture (Fig. 4*B*) and displayed a subpopulation of cells growing from underneath the tumor nodule, many of which displayed bright fluorescence (Fig. 4*C*). Any nonfluorescent cells that were observed likely represent stromal cells that were recovered when the tumor nodule was isolated. These data indicate that after 3 months *in vivo*, cells retain high levels of Sod2-GFP expression with no apparent growth defect either *in vivo* or *in vitro* and seem to maintain their promigratory phenotype.

Sod2-enhanced migration is retained in HT-1080 lung metastases. To assess whether isolated tumor cells from pulmonary metastases, which retained Sod2-GFP expression *in vivo*, maintain a promigratory phenotype, the movement of the leading edge of cells that were observed to migrate from the tumor nodule was evaluated by time-lapse video microscopy. Figure 5*A* represents images clearly displaying a movement of cells at the leading edge over a 24-h time frame (see video, Supplementary

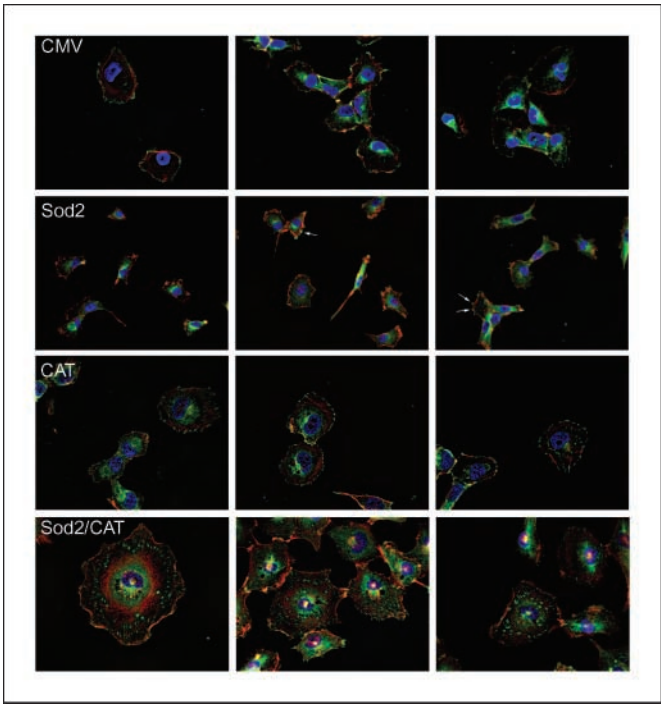

Figure 3. Sod2 expression leads to a loss of focal adhesions. HT-1080 cells stably transfected with empty vector (CMV), Sod2, CAT, or Sod2/CAT were incubated, fixed, and stained for vinculin (*green*), smooth muscle actin (*red*), and DNA (*blue*). *Arrows,* representative localized focal contacts.

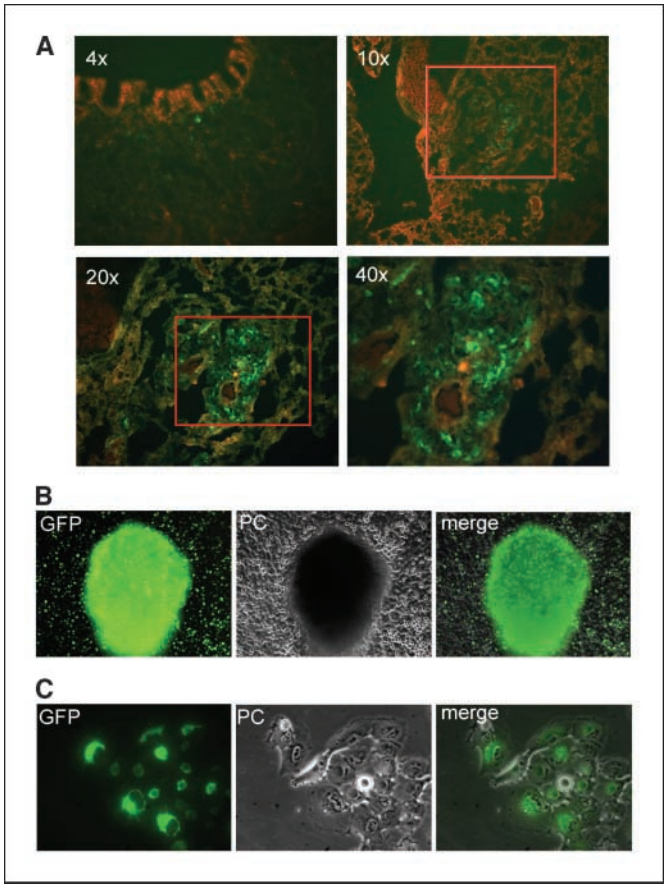

Figure 4. Metastatic pulmonary nodules retain fluorescence *in vivo* and *ex vivo*. Nude mice were injected with 1×10^6 HT-1080 fibrosarcoma cells overexpressing Sod2-GFP. After 2 mo, mice were sacrificed and lung cryosections analyzed for GFP under a fluorescent microscope. *A,* representative image of an intrapulmonary micrometastatic lesion surrounding a pulmonary capillary viewed under ×10, ×20, and ×40 magnifications. *B,* Sod2-GFP expression is retained in isolated mouse pulmonary lesions. Pulmonary lesions were isolated 2 mo following injection of high Sod2-GFP–expressing cell lines and cultured for 2 d in selective medium. Representative image of pulmonary metastatic node (×10 magnification) isolated from a Sod2-GFP–injected mouse, displaying the fluorescent image of the tumor in focal plane (GFP), the phase-contrast view of the underlying cell monolayer in focal plane (*PC*), and the merged image. *C,* representative image of the leading edge of the Sod2-GFP tumor-derived monolayer (×40 magnification), displaying the fluorescent image (*GFP*), phase-contrast view (*PC*), and merged image.

data). It was observed that the cells of the leading edge represented a nonuniform population with respect to Sod2 expression as assessed by GFP fluorescence. Therefore, it was possible to discriminate between cells expressing high levels of Sod2 (displaying bright GFP fluorescence) and low levels of Sod2 (displaying dim GFP fluorescence) and assess any differences that levels of Sod2 expression play on migration in these cells. The migratory activities of both bright and dim Sod2-GFP fluorescing cells were monitored over a 24-h time period (Fig. 5*B*), and it was observed that compared with the dim GFP cells, the bright cells showed higher activity of movement and traveled significantly farther (Fig. 5*B* and *C*). This further highlights that Sod2 enhances the migratory properties of HT-1080 cells, which seems to be dependent on Sod2 expression levels.

Pulmonary metastases retain high MMP-1 expression *in vivo*. Overexpression of Sod2 is associated with elevations in MMP-1 mRNA and protein production (16, 27). Analyzing MMP-1 production from cells that were sorted based on the levels of GFP fluorescence, it was found that low and high Sod2-expressing cell populations displayed increased MMP-1 expression, whereas GFP only–expressing cells showed no changes in MMP-1 expression compared with nontransfected cells (Fig. 6*A*). Accordingly, the high Sod2-GFP overexpressing cells had higher expression of MMP-1 than the low Sod2-GFP overexpressing cells, suggesting tight regulation of Sod2 on MMP-1 expression. This increase in MMP-1 levels was also observed in isolated pulmonary metastatic lesions derived from tail vein injections of Sod2-expressing HT-1080 cells (Fig. 6*B*). These data indicate that high *Sod2* and *MMP-1* gene expressions are maintained *in vivo*, aiding basement membrane degradation to further facilitate the formation of pulmonary metastatic lesions.

Further, this increase in MMP-1 levels following overexpression of Sod2 was shown to be a H_2O_2-dependent effect. Expression of MMP-1 was previously shown to be unaffected by overexpression of a catalytically inactive form of Sod2 (22), and real-time reverse transcription-PCR (RT-PCR) data from redox engineered cell lines show that overexpression of CAT and mitochondrially targeted CAT significantly decreases the induced MMP-1 expression observed in Sod2-GFP^{hi} HT-1080 cells (Fig. 6*C*). Contrary to the striking effects on MMP-1 mRNA levels on CAT overexpression, levels of tissue inhibitors of metalloproteinases (TIMP-1 and TIMP-2) were only marginally affected by CAT (Fig. 6*C*), suggesting that the effects on MMP-1 expression are primarily due to direct effects of Sod2 via H_2O_2 on *MMP-1* transcription.

Discussion

ROS have long been associated with neoplastic transformation either by alterations resulting in mutagenic DNA sequence changes or through activation of oncogenes and/or the inactivation of tumor suppressor genes (28–30). Additional to these events is the inherent ability of the tumor to maintain an increased free radical load without succumbing to the toxicity associated with ROS production (31, 32). This increased free radical load may arise either from a decrease in the ability of cells to detoxify ROS or from an increase in their ROS-generating capacity. In recent years, it has become more evident that ROS are not merely toxic by-products of metabolism but also serve an important regulatory role in numerous oncogenic signaling pathways (8, 29, 33, 34).

In vitro studies have shown that a number of cancer cells contain elevated levels of Sod and that this correlates with increased metastasis, proliferation, and resistance to apoptosis (16, 35–37). In addition, a reduction in CAT activity has been shown to correlate with an increase in the malignant phenotype (34). Mice that are deficient in their ability to detoxify H_2O_2, as a result of the loss of the antioxidant enzyme CAT, develop spontaneous mammary tumors at an early age relative to control mice (38). These observations are consistent with the finding that steady-state H_2O_2 levels are increased in many tumor cell lines, representing a variety of tissue types (23, 32, 39, 40).

It has become clear that manipulating the cellular redox state with Sod2 can have diverse effects on the malignant phenotype depending on the level of redox modulation, the tumor cell line being studied, the underlying oncogenic mutation, and the stage of disease progression. Thus, it is difficult to predict how tumors will respond to increases in steady-state production of H_2O_2 due to their heterogeneic makeup. The idea that increases in Sod2

potentiate the malignant phenotype contradicts many reports showing that Sod2 is a putative tumor suppressor. The role of Sod2 as a tumor suppressor is based on studies from numerous groups indicating that the levels of Sod2 are low in tumor tissue when compared with normal tissue, and is further substantiated by the ability of Sod2 overexpression to inhibit the growth of many tumor cell types both *in vitro* and *in vivo*. We refer the reader to comprehensive reviews on this topic (39, 40). In addition, Sod2-plasmid liposomes have been shown to be effective in enhancing the killing of orthotopic lung and oral tumors in response to ionizing radiation while protecting normal tissue (41, 42). Epperly et al. (41) have shown that squamous cell carcinomas are much more susceptible to toxicity of H_2O_2 than are primary fibroblast cultures. The authors also show that the antioxidant scavenging pool is more severely depleted in tumor tissue relative to normal tissue in response to *Sod2*-plasmid liposome treatment and irradiation. It is likely that increases in oxidant production in response to ionizing radiation and Sod2 may reach a threshold that exceeds the oxidant scavenging capacity of the tumor, leading to its demise. Our findings indicate that modulating the steady-state production of H_2O_2, below a toxic threshold, through antioxidant enzyme manipulation can affect the migratory capacity of tumor cells and their ability to modify the extracellular matrix microenvironment. Alterations in the rate of H_2O_2 production to that of its removal may be correlated with the development of malignant disease. In agreement with this observation, we show that Sod2-GFP–expressing cells leaving the leading edge of isolated pulmonary metastatic lesions are more migratory. We have previously shown that in cells expressing Sod2-GFP, GFP fluorescence intensity correlates with Sod2 activity (21, 23), and it is evident in the present study that the level of migration was correlated to the amount of Sod2 activity in these cells.

An integral part of migration and adhesion is the dynamic rearrangement of focal adhesion complexes in the cell. In the present study, we observed a loss of globally distributed mature focal adhesions, yet observed the presence of focal complexes in our motile redox engineered cells, implicating Sod2 in the disruption of mature focal adhesion formation, yet contributing to active remodeling of focal complexes of the lamellipodia required for migration. It has been shown that ROS modulate Rac and Rho signaling, which are important regulators of cytoskeletal dynamics, contributing to a loss of adhesion and a transition to a migratory phenotype (3, 5, 43).

The ability of tumor cells to migrate and invade through the extracellular matrix is, in part, attributed to its ability to remodel and degrade the extracellular matrix. MMPs have been shown to play an important role in extracellular proteolysis, facilitating migration and invasion, and have been extensively associated with tumor progression and metastasis (11–13). Previously, we showed that Sod2 expression increased MMP levels and that this corresponded with increased invasiveness (16). Therefore, we sought to further identify a potential correlation between the Sod2 status of these cells and their invasive phenotype including MMP-1 protein expression. In tumor nodes resected from mice, elevated Sod2 expression was associated with an increase in MMP-1 levels when compared with control cells. In addition, in Sod2-GFP cells sorted based on GFP fluorescence, MMP-1 activity corresponded to increases in Sod2 activity.

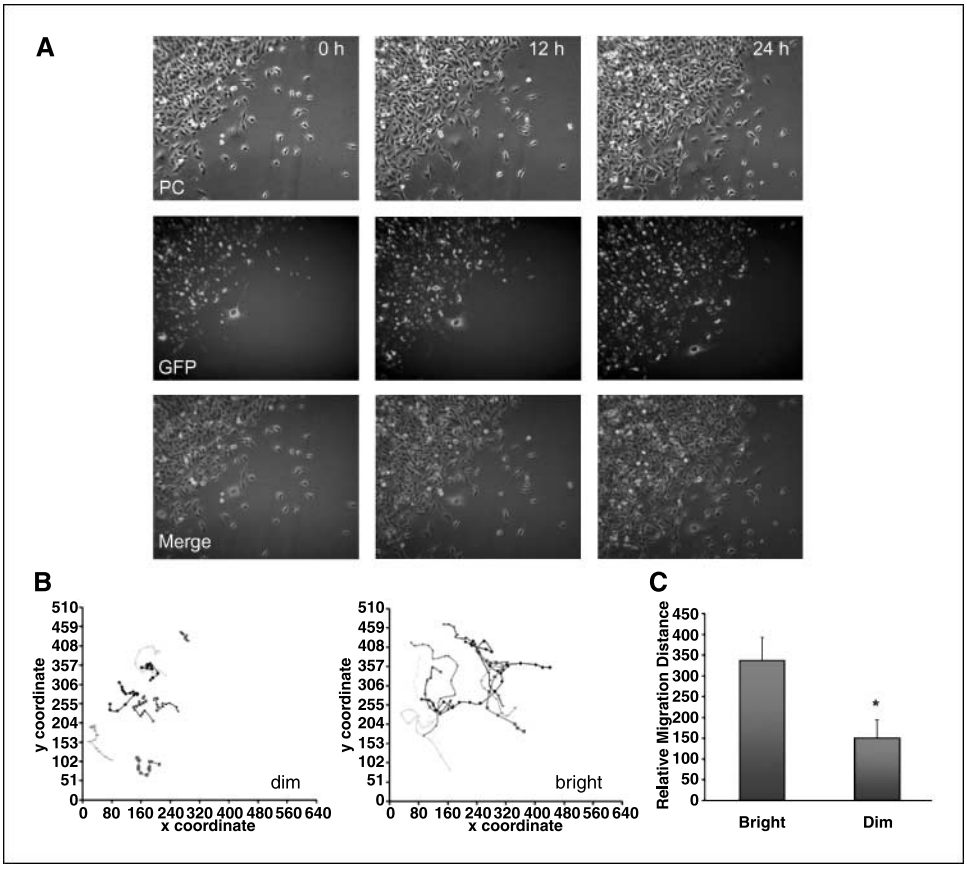

Figure 5. Quantification of time-lapse video microscopy. *A,* resected pulmonary tumor nodule from a nude mouse was allowed to grow in culture and cells at the leading edge of the tumor were analyzed for movement. Representative phase-contrast (PC), fluorescent (GFP), and merged images of Sod2-GFP cell movement at zero, 12-, and 24-h time points (see Supplementary video for movement over a 24-h period). *B,* migration of nine dimly and nine brightly fluorescing cells were tracked during time-lapse video microscopy for 24 h. Fluorescing cells were tracked for movement through the *x* and *y* coordinates using Image J software. *C,* brightly fluorescing cells display statistically more movement through the *x* and *y* coordinates than do dim fluorescing cells. *, $P \leq 0.05$.

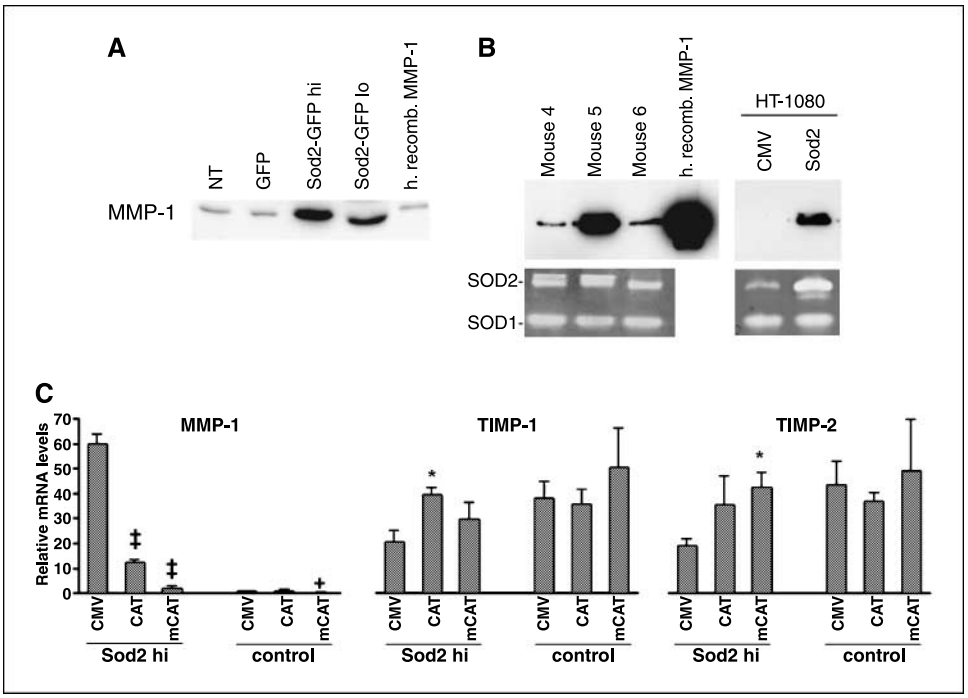

Figure 6. MMP-1 protein expression is increased in metastatic lesions displaying high Sod2 activity. *A,* MMP-1 expression correlates to Sod2 activity in HT-1080 cells. Nontransfected (*NT*) HT-1080 cells, HT-1080 cells transfected with GFP, and cells transfected with Sod2-GFP, which were sorted into low and high Sod2-expressing populations by fluorescence-activated cell sorting, were analyzed for MMP-1 protein expression. Secreted MMP-1 was immunoprecipitated from conditioned cell media and the proteins were separated on 10% SDS-PAGE, followed by Western blotting for MMP-1. *B,* pulmonary metastatic lesions derived from HT-1080 cells retain Sod2 and MMP-1 expression *in vivo*. Nude mice were tail vein injected with 1×10^6 stably transfected Sod2-GFP HT-1080 fibrosarcoma cells. Mice were sacrificed after 2 mo and pulmonary tumors isolated. Tumors from three different mice were lysed, proteins quantified, and lysates resolved on 10% SDS-PAGE, followed by immunoblotting for MMP-1. Tumor lysates were resolved on a nondenaturing gel for Sod zymography as described in Materials and Methods. *C,* stably transfected HT-1080 cells expressing high Sod2 (*Sod2 hi*) or empty vector (*control*) were cotransfected with CMV, CAT, or mitochondrially targeted CAT (*mCAT*). RNA was isolated and reverse transcribed, and real-time RT-PCR for MMP-1, TIMP-1, and TIMP-2 was carried out. *, $P < 0.05$; $^+$, $P < 0.01$; ‡, $P < 0.0005$, significant differences in expression of mRNAs compared with control cells (CMV) using Student's *t* test ($n = 3$).

The *Sod2* polymorphism at codon 16, which converts a valine to alanine in the mitochondrial targeting sequence of the protein, has been linked to clinically significant increases in both breast and prostate cancers in populations with a poor dietary antioxidant status (9, 10, 44). The Val→Ala transition alters the secondary structure of the protein, allowing for more efficient mitochondrial import and an increase in activity (45, 46). In heavy smokers, the Ala polymorphism is significantly associated with increased risk of developing high-grade prostate tumors (44). It has been hypothesized that deficiencies in nutritional antioxidants may exacerbate damage associated with the increased production of H_2O_2 resulting from the enhanced activity of Sod2. A variety of epidemiologic studies have also linked increases in Sod2 levels, independent of polymorphism, with significant increases in colon, gastric, lung, and breast cancers, as well as mesothelioma and glioblastoma (7, 39, 47–51). Of these studies, the increases in Sod2 activity or mRNA from tumor to normal tissue vary. Ray et al. (7) reported a 1.66-fold increase in Sod activity from patients with stage II, which remained high in both stage III and IV disease. Toh et al. (51) reported 2.19- and 3.72-fold increases in Sod2 mRNA expression relative to normal tissue in gastric and colorectal cancers, respectively. Oncomine analysis reveals a consistent, statistically significant ($P < 0.01$) increase in Sod2 mRNA levels, which correlates with tumor stage and grade in brain, breast, bladder, and lung cancers.[5] Our findings indicate that a 2- to 4-fold increase in Sod2 activity, which is representative of changes in the human population, is sufficient to enhance the migratory phenotype (Fig. 2*C*) and increase MMP-1 expression (Fig. 6*A*) in HT-1080 fibrosarcoma cells. Thus, there exists a strong association between disease incidence, poor prognosis, and levels of Sod2.

Our findings provide mechanistic insight into the epidemiologic link between enhanced Sod2 activity and poor prognosis in many patient cancers. Increases in Sod2 activity enhance the invasive and migratory phenotype of tumor cells in a H_2O_2-dependent fashion. In addition, the Sod2-dependent production of H_2O_2 increases the expression of the matrix-degrading metalloproteinase MMP-1, which can alter the tumor/stromal microenvironment and thus create a permissive environment for metastatic disease. Overall, these findings suggest that effective and targeted H_2O_2 detoxification may serve to prevent activation of the molecular triggers that drive the invasive/migratory phenotype.

Acknowledgments

Received 4/3/2007; revised 6/22/2007; accepted 8/21/2007.

Grant support: Philip Morris USA, Inc., Philip Morris International, Public Health Service grants CA77068 and CA095011 (J.A. Melendez), and NIH Predoctoral Fellowship AI49822 (K.M. Connor).

The costs of publication of this article were defrayed in part by the payment of page charges. This article must therefore be hereby marked *advertisement* in accordance with 18 U.S.C. Section 1734 solely to indicate this fact.

We thank Xiao Fang Ha for her technical support.

[5] www.oncomine.org

References

1. Liotta LA, Stetler-Stevenson WG. Tumor invasion and metastasis: an imbalance of positive and negative regulation. Cancer Res 1991;51:5054–9s.
2. Stetler-Stevenson WG, Aznavoorian S, Liotta LA. Tumor cell interactions with the extracellular matrix during invasion and metastasis. Annu Rev Cell Biol 1993; 9:541–73.
3. Nimnual AS, Taylor LJ, Bar-Sagi D. Redox-dependent down-regulation of Rho by Rac. Nat Cell Biol 2003;5: 236–41.
4. Kheradmand F, Werner E, Tremble P, Symons M, Werb Z. Role of Rac1 and oxygen radicals in collagenase-1 expression induced by cell shape change. Science 1998; 280:898–902.
5. van Wetering S, van Buul JD, Quik S, et al. Reactive oxygen species mediate Rac-induced loss of cell-cell adhesion in primary human endothelial cells. J Cell Sci 2002;115:1837–46.
6. Ben Mahdi MH, Andrieu V, Pasquier C. Focal adhesion kinase regulation by oxidative stress in different cell types. IUBMB Life 2000;50:291–9.
7. Ray G, Batra S, Shukla NK, et al. Lipid peroxidation, free radical production and antioxidant status in breast cancer. Breast Cancer Res Treat 2000;59:163–70.
8. Punnonen K, Ahotupa M, Asaishi K, Hyoty M, Kudo R, Punnonen R. Antioxidant enzyme activities and oxidative stress in human breast cancer. J Cancer Res Clin Oncol 1994;120:374–7.
9. Ambrosone CB, Freudenheim JL, Thompson PA, et al. Manganese superoxide dismutase (MnSOD) genetic polymorphisms, dietary antioxidants, and risk of breast cancer [In Process Citation]. Cancer Res 1999;59:602–6.
10. Li H, Kantoff PW, Giovannucci E, et al. Manganese superoxide dismutase polymorphism, prediagnostic antioxidant status, and risk of clinical significant prostate cancer. Cancer Res 2005;65:2498–504.
11. Nelson KK, Melendez JA. Mitochondrial redox control of matrix metalloproteinases. Free Radic Biol Med 2004;37:768–84.
12. Nabeshima K, Inoue T, Shimao Y, Sameshima T. Matrix metalloproteinases in tumor invasion: role for cell migration. Pathol Int 2002;52:255–64.
13. Matrisian LM. The matrix-degrading metalloproteinases. BioEssays 1992;14:455–63.
14. Durko M, Navab R, Shibata HR, Brodt P. Suppression of basement membrane type IV collagen degradation and cell invasion in human melanoma cells expressing an antisense RNA for MMP-1. Biochim Biophys Acta 1997;1356:271–80.
15. Poola I, DeWitty RL, Marshalleck JJ, Bhatnagar R, Abraham J, Leffall LD. Identification of MMP-1 as a putative breast cancer predictive marker by global gene expression analysis. Nat Med 2005;11:481–3.
16. Nelson KK, Ranganathan AC, Mansouri J, et al. Elevated sod2 activity augments matrix metalloproteinase expression: evidence for the involvement of endogenous hydrogen peroxide in regulating metastasis. Clin Cancer Res 2003;9:424–32.
17. Ranganathan AC, Nelson KK, Rodriguez AM, et al. Manganese superoxide dismutase signals matrix metalloproteinase expression via H_2O_2-dependent ERK1/2 activation. J Biol Chem 2001;276:14264–70.
18. Zhang HJ, Zhao W, Venkataraman S, et al. Activation of matrix metalloproteinase-2 by overexpression of manganese superoxide dismutase in human breast cancer MCF-7 cells involves reactive oxygen species. J Biol Chem 2002;277:20919–26.
19. Yang JQ, Zhao W, Duan H, et al. v-Ha-RaS oncogene up-regulates the 92-kDa type IV collagenase (MMP-9) gene by increasing cellular superoxide production and activating NF-κB. Free Radic Biol Med 2001;31:520–9.
20. Bai J, Rodriguez AM, Melendez JA, Cederbaum AI. Overexpression of catalase in cytosolic or mitochondrial compartment protects HepG2 cells against oxidative injury. J Biol Chem 1999;274:26217–24.
21. Rodriguez AM, Carrico PM, Mazurkiewicz JE, Melendez JA. Mitochondrial or cytosolic catalase reverses the MnSOD-dependent inhibition of proliferation by enhancing respiratory chain activity, net ATP production, and decreasing the steady state levels of H(2)O(2). Free Radic Biol Med 2000;29:801–13.
22. Nelson KK, Subbaram S, Connor KM, et al. Redox-dependent matrix metalloproteinase-1 expression is regulated by JNK through Ets and AP-1 promoter motifs. J Biol Chem 2006;281:14100–10.
23. Connor KM, Subbaram S, Regan KJ, et al. Mitochondrial H_2O_2 regulates the angiogenic phenotype via PTEN oxidation. J Biol Chem 2005;280:16916–24.
24. Dabiri G, Campaner A, Morgan JR, Van De Water L. A TGF-β1-dependent autocrine loop regulates the structure of focal adhesions in hypertrophic scar fibroblasts. J Invest Dermatol 2006;126:963–70.
25. Melendez JA, Davies KJA. Manganese superoxide dismutase modulates interleukin-1a levels in HT-1080 fibrosarcoma cells. J Biol Chem 1996;271:18898–903.
26. Melendez JA, Melathe RP, Rodriguez AM, Mazurkiewicz JE, Davies KJA. Nitric oxide enhances the manganese superoxide dismutase-dependent suppression of proliferation in HT-1080 fibrosarcoma cells. Cell Growth Differ 1999;10:655–64.
27. Ranganathan AC, Nelson KK, Rodriguez AM, et al. Manganese superoxide dismutase signals matrix metalloproteinase expression Via H_2O_2-dependent ERK1,2 activation. J Biol Chem 2001;276:14264–70.
28. Feig DI, Reid TM, Loeb LA. Reactive oxygen species in tumorigenesis. Cancer Res 1994;54:1890–4s.
29. Kong Q, Beel JA, Lillehei KO. A threshold concept for cancer therapy. Med Hypotheses 2000;55:29–35.
30. Breimer LH. Molecular mechanisms of oxygen radical carcinogenesis and mutagenesis: the role of DNA base damage. Mol Carcinog 1990;3:188–97.
31. Cerutti PA. Prooxidant states and tumor promotion. Science 1985;227:375–81.
32. Szatrowski TP, Nathan CF. Production of large amounts of hydrogen peroxide by human tumor cells. Cancer Res 1991;51:794–8.
33. Bai J, Cederbaum AI. Overexpression of catalase in the mitochondrial or cytosolic compartment increases sensitivity of HepG2 cells to tumor necrosis factor-α-induced apoptosis. J Biol Chem 2000;275:19241–9.
34. Gupta A, Butts B, Kwei KA, et al. Attenuation of catalase activity in the malignant phenotype plays a functional role in an *in vitro* model for tumor progression. Cancer Lett 2001;173:115–25.
35. Dasgupta J, Subbaram S, Connor KM, et al. Manganese superoxide dismutase protects from TNF-α-induced apoptosis by increasing the steady-state production of H(2)O(2). Antioxid Redox Signal 2006;8: 1295–305.
36. Kahlos K, Soini Y, Paakko P, Saily M, Linnainmaa K, Kinnula VL. Proliferation, apoptosis, and manganese superoxide dismutase in malignant mesothelioma. Int J Cancer 2000;88:37–43.
37. Nonaka Y, Iwagaki H, Kimura T, Fuchimoto S, Orita K. Effect of reactive oxygen intermediates on the *in vitro* invasive capacity of tumor cells and liver metastasis in mice. Int J Cancer 1993;54:983–6.
38. Nishikawa M, Tamada A, Kumai H, Yamashita F, Hashida M. Inhibition of experimental pulmonary metastasis by controlling biodistribution of catalase in mice. Int J Cancer 2002;99:474–9.
39. Kinnula VL, Crapo JD. Superoxide dismutases in malignant cells and human tumors. Free Radic Biol Med 2004;36:718–44.
40. Oberley LW. Mechanism of the tumor suppressive effect of MnSOD overexpression. Biomed Pharmacother 2005;59:143–8.
41. Epperly MW, Wegner R, Kanai AJ, et al. Effects of MnSOD-plasmid liposome gene therapy on antioxidant levels in irradiated murine oral cavity orthotopic tumors. Radiat Res 2007;167:289–97.
42. Epperly MW, Defilippi S, Sikora C, Gretton J, Kalend A, Greenberger JS. Intratracheal injection of manganese superoxide dismutase (MnSOD) plasmid/liposomes protects normal lung but not orthotopic tumors from irradiation. Gene Ther 2000;7:1011–8.
43. Wu RF, Xu YC, Ma Z, Nwariaku FE, Sarosi GA, Jr., Terada LS. Subcellular targeting of oxidants during endothelial cell migration. J Cell Biol 2005; 171:893–904.
44. Woodson K, Tangrea JA, Lehman TA, et al. Manganese superoxide dismutase (MnSOD) polymorphism, α-tocopherol supplementation and prostate cancer risk in the α-tocopherol, β-carotene cancer prevention study (Finland). Cancer Causes Control 2003;14:513–8.
45. Sutton A, Khoury H, Prip-Buus C, Cepanec C, Pessayre D, Degoul F. The Ala16Val genetic dimorphism modulates the import of human manganese superoxide dismutase into rat liver mitochondria. Pharmacogenetics 2003;13:145–57.
46. Sutton A, Imbert A, Igoudjil A, et al. The manganese superoxide dismutase Ala16Val dimorphism modulates both mitochondrial import and mRNA stability. Pharmacogenet Genomics 2005;15:311–9.
47. Ho JCM, Zheng S, Comhair SAA, Farver C, Erzurum SC. Differential expression of manganese superoxide dismutase and catalase in lung cancer. Cancer Res 2001; 61:8578–85.
48. Izutani R, Katoh M, Asano S, Ohyanagi H, Hirose K. Enhanced expression of manganese superoxide dismutase mRNA and increased TNFα mRNA expression by gastric mucosa in gastric cancer. World J Surg 1996;20: 228–33.
49. Satomi A, Murakami S, Hashimoto T, Ishida K, Matsuki M, Sonoda M. Significance of superoxide dismutase (SOD) in human colorectal cancer tissue: correlation with malignant intensity. J Gastroenterol 1995;30:177–82.
50. Tsanou E, Ioachim E, Briasoulis E, et al. Immunohistochemical expression of superoxide dismutase (MnSOD) anti-oxidant enzyme in invasive breast carcinoma. Histol Histopathol 2004;19:807–13.
51. Toh Y, Kuninaka S, Oshiro T, et al. Overexpression of manganese superoxide dismutase mRNA may correlate with aggressiveness in gastric and colorectal adenocarcinomas [In Process Citation]. Int J Oncol 2000;17:107–12.